



Impact of annealing on martensitic transformation of $\text{Mn}_{50}\text{Ni}_{42.5}\text{Sn}_{7.5}$ shape memory alloy

T. Bachaga^{1,2,3} · J. Zhang¹ · S. Ali¹ · J. J. Sunol³ · M. Khitouni²

Received: 25 September 2018 / Accepted: 5 January 2019 / Published online: 1 February 2019
© Springer-Verlag GmbH Germany, part of Springer Nature 2019

Abstract

The impact of annealing on the structural and martensitic transformation of $\text{Mn}_{50}\text{Ni}_{42.5}\text{Sn}_{7.5}$ (at.%) shape memory alloy was systematically investigated using a scanning electron microscope, X-ray diffraction (XRD), and differential scanning calorimetry. Analysis of X-ray diffraction patterns confirms that the as-cast and annealed alloys have martensitic structure at room temperature: seven-layered monoclinic 14M. In addition, it has observed that during annealing, the transition temperatures have increased relative to the cast alloy. Also, a high dependence between the cooling rate and activation energy has detected. A more detailed characterization of martensitic transition and account of thermodynamic parameters were examined after annealing.

1 Introduction

Heusler-based Mn–Ni shape memory alloys have received increasing interest in technological applications, due to their potential functional properties during martensitic transformation (MT). This transition is from a cubic austenitic phase $L2_1$ or B2 at high temperature to a martensitic phase, whose structure can be $L1_0$, 10M and 14M at low temperature [1–4]. Their properties make them a particular point of interest for the development of new magnetically driven actuators, sensors and coolers for magnetic refrigeration [5]. The Mn–Ni–Sn system has prospective importance as a shape memory alloy. Recently, researchers have examined the physical properties of Heusler alloys $\text{Mn}_{50}\text{Ni}_{50-x}\text{Sn}_x$ system. Coll et al. [6] showed that this system has a unique austenitic of cubic structure and that it transforms into a martensitic phase of different structures with modulation during cooling. The Heusler $\text{Mn}_{50}\text{Ni}_{50-x}\text{Sn}_x$ alloys showed a

large magnetic entropy change [7, 8], a significant exchange bias field [9], and a slight thermal delay [10] during the martensitic change. Lately, important reports on the effect of annealing on similar alloys have been distributed. Schagel et al. [11] investigated the effect of annealing on the martensitic phase transformation temperatures in $\text{Ni}_{50}\text{Mn}_{50-x}\text{Sn}_x$ alloys at different cooling rates. The effect of annealing on the martensitic transformation of $\text{Ni}_{44.1}\text{Mn}_{44.2}\text{Sn}_{11.7}$ ribbons was examined by Xuan et al. [12]. They showed that with different annealing temperatures, the MT of the annealed ribbons increases obviously. On the other hand, Fichtner et al. [13] announced that the annealing of alloys resulted in a decrease in martensitic transformation temperatures and an expansion in thermal hysteresis during a martensitic transformation. This could be related to a release of stress during the annealing process. In addition, Liu et al. [14] showed that during an increase in quenching speed of the bulk $\text{Co}_{46}\text{Ni}_{27}\text{Ga}_{27}$ alloy, the martensitic transformation temperature increases monotonically. Also, Sarma et al. [15] found the same correlation for $\text{Co}_{47}\text{Ni}_{23}\text{Ga}_{30}$ ingots. At present, no studies on the effect of annealing on the martensitic transformation of $\text{Mn}_{50}\text{Ni}_{42.5}\text{Sn}_{7.5}$ (at.%) alloy have been performed. Thus, the purpose of this study is to investigate the impact of annealing on the modification of the microstructure and the behavior of phase transformation temperatures of Heusler $\text{Mn}_{50}\text{Ni}_{42.5}\text{Sn}_{7.5}$ (at.%) alloy.

✉ T. Bachaga
bachagatarak@yahoo.fr

✉ J. Zhang
zhangjh_radicat@163.com

¹ School of Computer Sciences and Technology, University of Qingdao, Qingdao, China

² Laboratory of Inorganic chemistry, UR-11-ES-73, University of Sfax, 3000 Sfax, Tunisia

³ Dep. de Física, Universitat de Girona, Campus Montilivi, 17071 Girona, Spain

2 Experimental

An as-cast ingot with a nominal composition of $\text{Mn}_{50}\text{Ni}_{42.5}\text{Sn}_{7.5}$ (at.%) was prepared by arc melting from a Ni metal filament (purity > 99.98%), metallic manganese sheets (purity > 99.98%) and pieces of metallic Sn in the form of small spheres (purity > 99.99%), using Buhler MAM-1 compact arc melting under an argon atmosphere. The mass of the ingot prepared by arc melting was ~ 4 g. An extra 5 wt% Mn was added to compensate for evaporation losses. The bulk alloy was melted four times, to ensure the homogeneity of the chemical composition. In our case, to better ensure the recycling of Mn and control the composition, the elements were placed increasingly according to their melting temperatures more precisely, Sn ($T_f = 231$ °C) the lowest, Mn ($T_f = 1246$ °C) and finally the highest Ni ($T_f = 1455$ °C). The bulk alloy was fixed in a quartz tube filled with argon gas, followed by annealing

at 1273 K for 1 h, and then quenched in ice water. Following that, the obtained samples are named as-cast and annealed. Their microstructures and chemical compositions were determined by scanning electron microscopy (SEM) using a ZEISS DSM-960A microscope operated at 30 kV and linked with an energy-dispersive spectrometry (EDX) attachment. The mean grain size was measured from SEM images of as-cast and annealed samples by ImageJ software. The structural characterization of the samples at room temperature (RT) was performed by X-ray diffractometer (XRD), using a Siemens D500 X-ray powder diffractometer with $\text{Cu-K}\alpha$ radiation ($\lambda = 1.5418$ Å). XRD refinement analysis was performed by applying Rietveld method and Jana software [16]. The calorimetric measurements were performed by a Mettler–Toledo differential scanning calorimetry (DSC) 822 in a flowing argon atmosphere. DSC curves were determined at different cooling rates, to calculate the activation energy by Kissinger method.

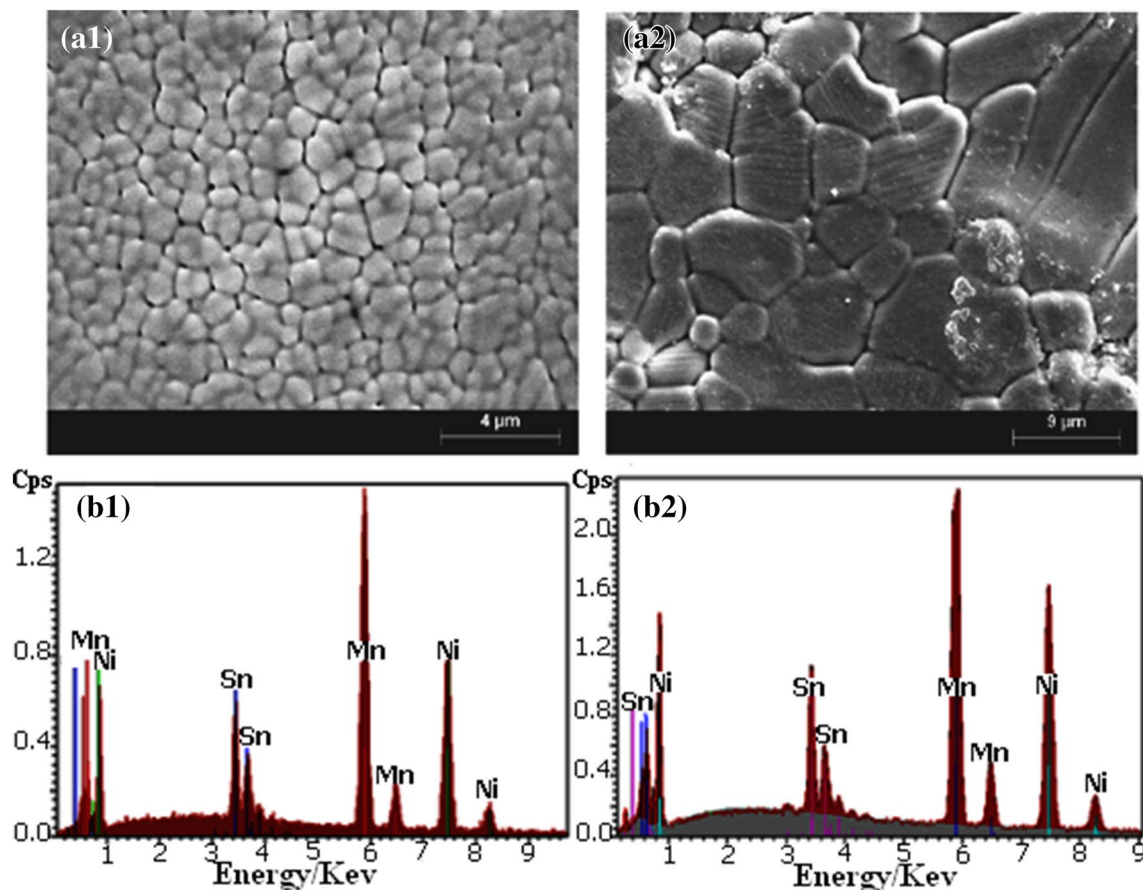


Fig. 1 Typical SEM micrographs of $\text{Mn}_{50}\text{Ni}_{42.5}\text{Sn}_{7.5}$ alloy: **a** as-cast, **b** annealed

3 Results and discussion

Figure 1 shows the micrographs of as-cast and annealed samples. The granular microstructure of the as-cast ingot is illustrated in Fig. 1a1, where the average grain size of about 1.7 μm is observed. As shown in Fig. 1b1, the average grain size increased to reach 6.6 μm after annealing. It is obvious that there is an increase in grain sizes after annealing of the alloy. Some EDX measurements were performed on each alloy surface to check the homogeneity of the final composition. The standard deviation obtained for the elemental chemical composition (as determined by EDX) was 0.4–0.6 at.% for Mn, 0.4–0.6 at.% for Ni, and 0.3–0.5 at.% for Sn. The EDX analysis of the as-cast and annealed samples is shown in Fig. 1a2, b2. The results confirm the presence of the metallic mixture. The composition analysis was found to be in good agreement with the nominal compositions of the as-cast and annealed alloys: [(49.88 at.% Mn; 42.69 at.% Ni; 7.43 at.% Sn) and (49.33 at.% Mn; 43.22 at.% Ni; 7.45 at.% Sn)]. The compositions shifted from the original. This is usual in the alloys obtained by arc melting followed by annealing. To back the results from the microstructure analysis of both alloys, XRD analysis was performed. X-ray diffraction patterns of both the alloys recorded at room temperature are shown in Fig. 2. All the Bragg peaks are sharp and will be indexed as a modulated monoclinic (14M) martensite. The structure of martensite obtained in both alloys is identical to the structure observed in melt spun ribbons

with similar composition [4]. It must be remarked that no detected secondary phase could be adjusted to the obtained XRD patterns. The structure of both alloys was almost identical, except for slight differences in the peak intensities and angles, suggesting a decrease in cell volume. The structural parameters are shown in Table 1. Miller indexes were doled out with the guide of ordering programs as Treor and Dicvol. Furthermore, it is seen clearly that the diffraction peaks become narrower in both alloys, indicating that the grain sizes of annealed alloy increase, which is consistent with the SEM results. In addition, it should be noted that the diffraction peaks of the samples fade slightly after annealing. This allows us to deduce that the grain sizes increases after annealing and reduces the Mn–Mn distance. Similar results have been found in other Heusler Ni₄₉Mn₃₉Sn₁₂ alloys [17].

Figure 3 shows the DSC curves of the as-cast and annealed samples. The characteristic transition temperatures (A_s , A_f , M_s and M_f) are determined. The beginning and end of the transformation temperatures were determined by selecting the intersection of a baseline and the tangents to each peak, as shown in Fig. 3. The phase transformation temperatures undergo a slight increase after annealing and the hysteresis width ($\Delta T = A_s - M_f$) shifts from 17 to 25 K, for the annealed sample. The reason for this change can be mainly attributed to the evolution of the atomic ratio of the electron (ea), the interatomic distance of Mn–Mn and the grain sizes. First, as indicated by Krenke et al. [18], the characteristic temperatures of the martensitic transition for the Ni–Mn–Sn system strongly depend on the electron

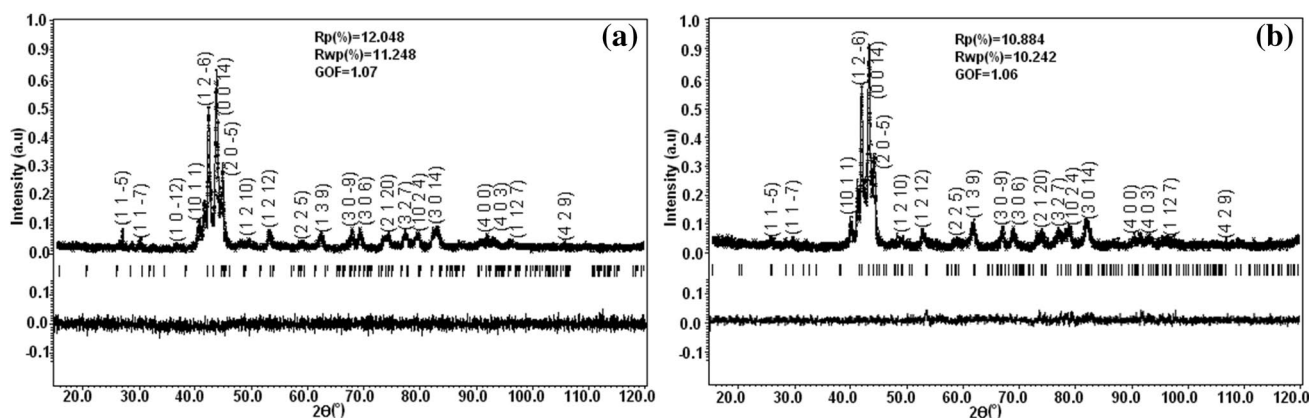


Fig. 2 The XRD patterns of Mn₅₀Ni_{42.5}Sn_{7.5} alloy: **a** as-cast, **b** annealed

Table 1 Refined unit cell parameters' values of Heusler Mn₅₀Ni_{42.5}Sn_{7.5} alloy

Mn ₅₀ Ni _{42.5} Sn _{7.5} alloy	Lattice parameters				
	<i>a</i> (Å)	<i>b</i> (Å)	<i>c</i> (Å)	β (°)	Volume (Å ³)
As-cast	4.3196 (3)	5.6109 (3)	29.9216 (2)	93.98	723.45 (2)
Annealed	4.3077 (3)	5.6003 (3)	29.8950 (2)	93.57	719.79 (2)

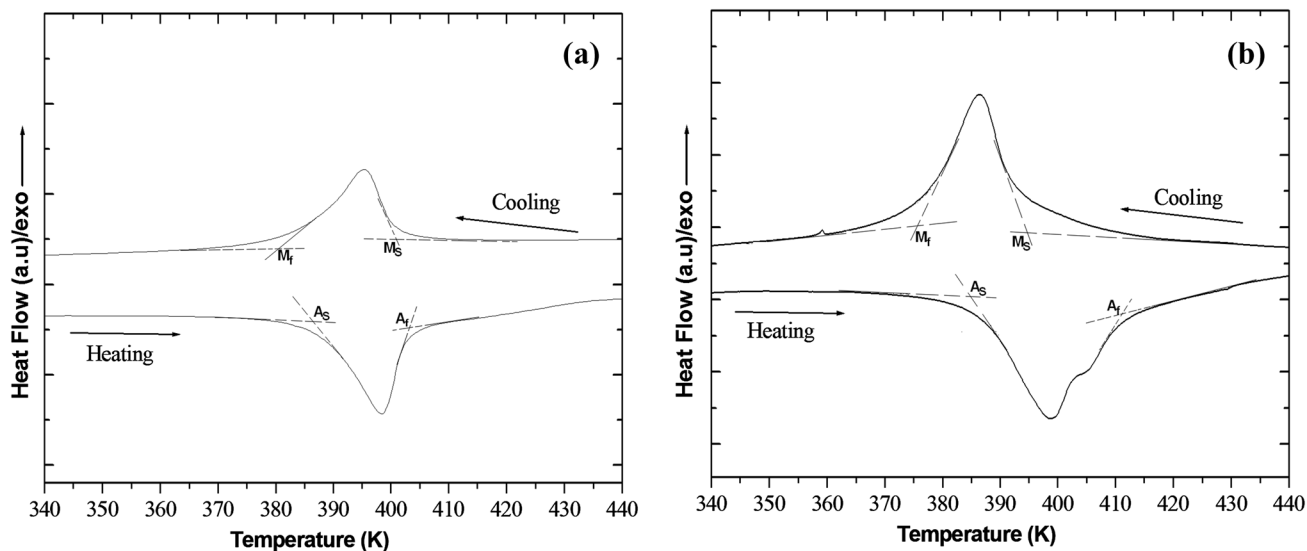


Fig. 3 DSC curves of $\text{Mn}_{50}\text{Ni}_{42.5}\text{Sn}_{7.5}$ alloy: **a** as-cast, **b** annealed

concentration (e/a). They showed that all these progression temperatures increase with the ratio (e/a). The values of this report in our work are 8.05 and 8.07, respectively. This increase in (e/a) values may be due to the volatilization of some manganese during annealing. Then, as another reason related to this change of martensitic transition temperatures, one can mark the effect of the distance of Mn–Mn. Buchelnikov et al. [19] showed that the site of the atom in the ingot is too stable and does not take an equilibrium position, during the rapid solidification from the liquid state to the solid state. After annealing, the alloy is subjected to a relaxation of the structure, which makes it possible to modify slightly the site of the atom, due to a change of the distance Mn–Mn. Finally, another justification for this change is the dependence between the annealing and grain size for annealed alloys observed in micrographs [20–22]. Glezer et al. [22] investigated the correlation between martensitic transition temperatures and grain size in Fe–Ni–B alloys. They noticed that these temperatures decreased with the decrease in grain size and that their critical grain size was smaller than that of the martensitic transformation during cooling.

From measurements obtained by DSC, we can examine the theory of martensitic transformation, specifically the activation energy E_a . The last parameter is the main parameter that must be obtained, to get the kinetic transformation of both the alloys. The Kissinger method for non-isothermal change was used to obtain the activation energy. In this case, the peak temperature T is used to determine the activation energy of two changes, since, it has discovered that the change was isokinetic.

Distinctive cooling rates running from 2 to $50^\circ\text{C min}^{-1}$ were used to make these measurements. Figure 4 shows the thermograms acquired for various cooling rates. It is

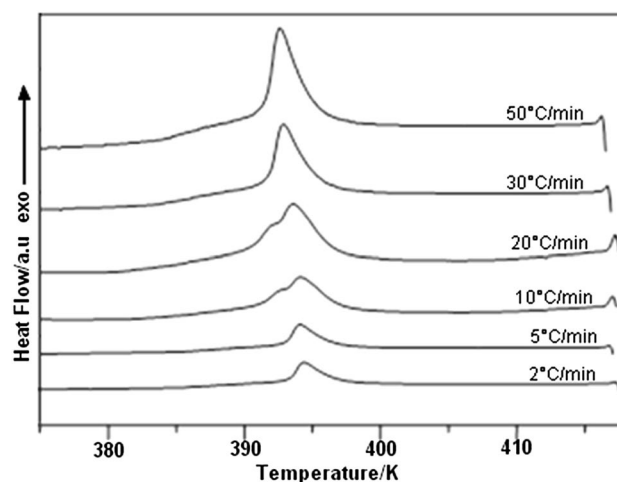


Fig. 4 DSC charts of annealed $\text{Mn}_{50}\text{Ni}_{42.5}\text{Sn}_{7.5}$ alloy recorded at different cooling rates

clear that the transition temperatures decrease with increasing cooling rates and that progress made with prolonged temperatures shows a propensity to expand with increasing cooling rate. Moreover, what is unique in our investigation of the $\text{Mn}_{50}\text{Ni}_{42.5}\text{Sn}_{7.5}$ sample is that two exothermic peaks can be observed during intermediate cooling rates. Previous studies had never detailed such an abnormal phenomenon [23, 24]. They proposed that, in addition to martensitic transformation, another inter-martensitic transformation happens between two martensitic phases of various structures. In this way, it is reasonable to consider the current transformation peaks in the DSC curve of the $\text{Mn}_{50}\text{Ni}_{42.5}\text{Sn}_{7.5}$ sample as a martensitic transformation and an inter-martensitic transformation, which are completely reversible and reproducible.

According to the data obtained from the DSC analysis, the maximum temperatures of the inter-martensitic transformations during the intermediate cooling rates 10 and 20 °C min⁻¹ are 393 and 391 K, respectively. The thermal activation energies of samples were carried out by DSC with different cooling rates of 2, 5, 10, 20, 30 and 50 °C min⁻¹ (Fig. 4). The purpose of calculating the activation energy is to determine the level of energy required by the sample during martensitic transformation. The Johnson–Mehl–Avrami (JMA) equation for solid-state transformation can be used to determine the activation energy of shape memory alloys as phase transformations occur. The JMA equation can be applied to a non-isothermal case. The Kissinger method is proposed for the analysis of non-isothermal activation energy of samples [25]. From JMA, the fraction X of the SMA_s after a given time t was indicated by the following equation:

$$X = 1 - \exp[-(Kt)^n], \quad (1)$$

where n is the Avrami exponent and K is the effective reaction rate usually assigned Arrhenius temperature dependence:

$$K = K_0 \exp(-E_a/RT). \quad (2)$$

The Kissinger method is one solution of Arrhenius equation. The activation energy can be calculated by applying the following equation according to the Kissinger method.

$$\ln(\beta/T^2) = A - E_a/RT, \quad (3)$$

where E_a is the activation energy, T is the maximum peak temperature of transition, R is the gas constant (8.314 J mol⁻¹), β is the cooling rate and A is the constant coefficient. Figure 5 shows the plot of $\ln(\beta/T^2)$ versus $1/T$. The values of the activation energy E_a for the annealed alloy were obtained from the slope of the line obtained by plotting $\ln(\beta/T^2)$ versus $1/T$. It is clear that there is a remarkable difference in activation energy for various scanning rates. The calculated values E_a are 259.604 and 12.215 kJ mol⁻¹,

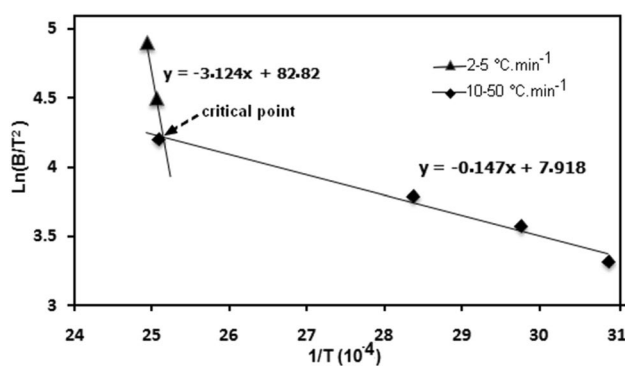


Fig. 5 The $\ln(\beta/T^2)$ vs. $1/T$ plot at different cooling rates of annealed Mn₅₀Ni_{42.5}Sn_{7.5} alloy

respectively. This difference in E_a leads to a dependence of the cooling rate and the activation energy E_a , where the high cooling rates and the low cooling rates correspond to very different activation energies. Meanwhile, over a wide range of rates (5–10 °C min⁻¹) between both the previous activation energies, the high values can slowly change to low values. This enables us to deduce that the critical point position is ~ 8 °C min⁻¹, as shown in Fig. 5. The kinetics of other alloys with first-order martensitic transformation, for example, Cu–Ni–Al [26], Fe–C(N) [27] and Ti–Al–V [28], as well as the ordering transition kinetics in the Ni–Mn–Ga alloy [29] were largely determined using the Kissinger method [30], based on colorimetric results. While, the scale rates are higher than 5 °C min⁻¹ in the previously mentioned literature, the work was limited to the rate dependence of the activation energy for lower speeds. Fernandez et al. [31] have shown that there seems to be, by all accounts, a critical point related to the slope of the linear curves of $\ln(\beta/T^2)$ with respect to $1/T$, and attributed this phenomenon to evaluated error. In the investigation of the Ni–Ti shape memory alloy, Hsu et al. [32] reported that the martensitic substructure could move from coarse twins to fine twins or stacking defects with cooling rates changing from 0.5 to 25 K min⁻¹. In addition, the atomic displacement of the stacking defects in the surface (0 0 1) with a high cooling rate is just a large part of that with a lower cooling rate. Therefore, the reason behind the rate dependence of activation energy in the present examination could probably be identified with the way that twinning and atomic displacements in the martensitic transformation process increase significantly at generally low cooling rates, which causes an increase in activation energy important for the progress. The speed of stage interfaces relies upon just the undercooling as the temperature rate reduces to low values [33]. Thus, the rapid cooling of the samples would promote greater undercooling in a generally short time during an examination with progressive cooling, which is responsible for a larger chemical driving force, and therefore lower activation energy. In this way, an example of rapid cooling would reinforce greater undercooling in a relatively short examination time, with step cooling, which is responsible for a greater synthetic main thrust, and along these lines for lower initiation vitality.

4 Conclusions

In summary, the impact of annealing on the microstructure, structural and martensitic transformation of Mn₅₀Ni_{42.5}Sn_{7.5} (at.%) shape memory alloy was studied. On the basis of the experimental results obtained, some conclusions can be cited.

- A martensite phase of a 14M modulated monoclinic structure was detected, at room temperature, for both alloys.
- The phase transformation temperatures increased remarkably after annealing.
- A high dependence between the cooling rates and the activation energy E_a has been detected.

Acknowledgements This work was funded by the “Taishan Scholar” Project of Shandong Province and Key Basic Research Project of Shandong Natural Science Foundation of China (no. ZR2017ZB0422).

References

1. T. Krenke, E. Duman, M. Acet, E.F. Wassermann, X. Moya, L. Mañosa, Magnetic superelasticity and inverse magnetocaloric effect in Ni–Mn–In. *Phys. Rev. B* **7575**, 104414 (2007)
2. T. Bachaga, R. Daly, L. Escoda, J.J. Suñol, M. Khitouni, Influence of chemical composition on martensitic transformation of MnNiIn shape memory alloys. *J. Therm. Anal. Calorim.* **122**, 167 (2015)
3. J.J. Sunol, L. Escoda, B. Hernando, J.L. Sanchez, V.M. Llamazares, Prida, Structural behavior of Ni–Mn–(In, Sn) Heusler melt spun ribbons. *J. ESOMAT* **2009**, 02031 (2009). <https://doi.org/10.1051/esomat/200902031>
4. T. Bachaga, R. Daly, M. Khitouni, L. Escoda, J. Saurina, J.J. Sunol, Thermal and structural analysis of Mn_{49.3}Ni_{43.7}Sn_{7.0} Heusler alloy ribbons. *Entropy* **17**, 646 (2015)
5. G. Yu, Y. Xu, Z. Liu, H. Qiu, Z. Zhu, X. Huang, L. Pan, Recent progress in Heusler-type magnetic shape memory alloys. *Rare Met.* **34**, 527 (2015)
6. R. Coll, L. Escoda, J. Saurina, J.L. Sanchez-Llamazares, B. Hernando, J.J. Sunol, Martensitic transformation in Mn–Ni–Sn Heusler alloys. *J. Therm. Anal. Calorim.* **99**, 905 (2010)
7. Z. Wu, Z. Liu, H. Yang, Y. Liu, G. Wu, Martensitic and magnetic transformation behaviors in Mn₅₀Ni_{42-x}Sn₈Co_x polycrystalline alloys. *J. Phys. D Appl. Phys.* **44**, 385403 (2011)
8. A. Ghosh, K. Mandal, Large magnetic entropy change and magnetoresistance associated with a martensitic transition of Mn-rich Mn_{50.5-x}Ni₄₁Sn_{8.5+x} alloys. *J. Phys. D Appl. Phys.* **46**, 435001 (2013)
9. L. Ma, W.H. Wang, J.B. Lu, J.Q. Li, C.M. Zhen, D.L. Hou, G.H. Wu, Coexistence of reentrant-spin-glass and ferromagnetic martensitic phases in the Mn₂Ni_{1.6}Sn_{0.4} Heusler alloy. *Appl. Phys. Lett.* **99**, 182507 (2011)
10. L. Ma, S.Q. Wang, Y.Z. Li, C.M. Zhen, D.L. Hou, W.H. Wang, J.L. Chen, G.H. Wu, Martensitic and magnetic transformation in Mn₅₀Ni_{50-x}Sn_x ferromagnetic shape memory alloys. *J. Appl. Phys.* **112**, 083902 (2012)
11. D.L. Schlagel, R.W. McCallum, T.A. Lograsso, Influence of solidification microstructure on the magnetic properties of Ni–Mn–Sn Heusler alloys. *J. Alloy. Compd.* **463**, 38 (2008)
12. H. Xuan, K. Xie, D. Wang, Z. Han, C. Zhang, B. Gu, Y. Du, Effect of annealing on the martensitic transformation and magnetocaloric effect in Ni_{44.1}Mn_{44.2}Sn_{11.7} ribbons. *Appl. Phys. Lett.* **92**, 242506 (2008)
13. T. Fichtner, C. Wang, A.A. Levin, G. Kreiner, C.S. Mejia, S. Fabbri, F. Albertini, C. Felser, effects of annealing on the martensitic transformation of Ni-based ferromagnetic shape memory heusler alloys and nanoparticles. *Metals* **5**, 484–503 (2015)
14. J. Liu, M. Xia, Y. Huang, H. Zheng, J. Li, Effect of annealing on the microstructure and martensitic transformation of magnetic shape memory alloys CoNiGa. *J. Alloy. Compd.* **417**, 96 (2006)
15. S. Sarma, A. Srinivasan, Influence of annealing temperature on the properties of Co–Ni–Ga ferromagnetic shape memory alloy. *Adv. Mater. Res.* **52**, 63 (2008)
16. V. Petrisek, D.M. Jana, *The Crystallographic Computing System* (Institute of Physics, Prague, 2000)
17. H. Zheng, D. Wu, S. Xue, J. Frenzel, G. Eggeler, Q. Zhai, Martensitic transformation in rapidly solidified Heusler Ni₄₉Mn₃₉Sn₁₂ ribbons. *Acta. Mater.* **59**, 5692 (2011)
18. T. Krenke, M. Acet, E.F. Wassermann, X. Moya, L. Manosa, Martensitic transitions and the nature of ferromagnetism in the austenitic and martensitic states of Ni–Mn–Sn alloys. *J. Phys. Rev. B* **72**, 014412 (2005)
19. V.D. Buchelnikov, S.V. Taskaev, M.A. Zagrebina, A.T. Zayak, T. Takagi, Phase transitions in Ni–Mn–Ga alloys with the account of crystal lattice modulation. *J. Mag. Mag. Mater.* **316**, 591 (2007)
20. T. Sánchez, J.L. Sánchez-Llamazares, B. Hernando, J.D. Santos, M.L. Sánchez, M.J. Pérez, J.J. Suñol, R. Sato, R. Grössinger, Annealing effect on martensitic transformation and magnetostructural properties of Ni–Mn–In melt spun ribbons. *Mater. Sci. Forum* **635**, 81–87 (2009)
21. M. Kaya, Y. Elerman, I. Dincer, Effect of heat treatment procedure on magnetic and magnetocaloric properties of Ni₄₃Mn₄₆In₁₁ melt spun ribbons. *Philos. Mag.* **98**, 1919–1932 (2018)
22. A.M. Glezer, E.N. Blinova, V.A. Pozdnyakov, A.V. Shelyakov, Martensite transformation in nanoparticles and nanomaterials. *J. Nanopart. Res.* **5**, 551–560 (2003)
23. H.X. Zheng, M.X. Xia, J. Liu, J.G. Li, Martensitic transformation of highly undercooled Ni–Fe–Ga magnetic shape memory alloys. *J. Alloy. Compd.* **385**, 144 (2004)
24. H.X. Zheng, J. Liu, M.X. Xia, J.G. Li, Martensitic transformation of Ni–Fe–Ga magnetic shape memory alloys. *J. Alloy. Compd.* **387**, 265 (2005)
25. H. Fang, B. Wong, Y. Bai, Kinetic modelling of thermophysical properties of shape memory alloys during phase transformation. *Const. Buil. Mater.* **131**, 146–155 (2017)
26. V. Recarte, J.I. Perez-Landazabal, A. Ibarra, M.L. No, J.S. Juan, High temperature β phase decomposition process in a Cu–Al–Ni shape memory alloy. *Mater. Sci. Eng. A* **378**, 238–242 (2004)
27. Z. Guo, W. Sha, D. Li, Quantification of phase transformation kinetics of 18 wt% Ni C250 maraging steel. *Mater. Sci. Eng. A* **373**, 10–20 (2004)
28. S. Malinov, Z. Guo, W. Sha, A. Wilson, Differential scanning calorimetry study and computer modeling of $\beta \rightarrow \alpha$ phase transformation in a Ti–6Al–4V alloy. *Metall. Mater. Trans. A* **32**, 879–887 (2001)
29. V. Sanchez-Alarcos, J.I. Perez-Landazabal, V. Recarte, J.A. Rodriguez-Velamazan, V.A. Chernenko, *J. Phys. Condens. Matter* **22**, 166001 (2010)
30. J. Vazquez, P. Villares, R. Jimenez-Garay, A theoretical method for deducing the evolution with time of the fraction crystallized and obtaining the kinetic parameters by DSC, using non-isothermal techniques. *J. Alloy. Compd.* **257**, 259 (1997)
31. J. Fernandez, A.V. Benedetti, J.M. Guilemany, X.M. Zhang, Thermal stability of the martensitic transformation of Cu–Al–Ni–Mn–Ti. *Mater. Sci. Eng. A* **438–440**, 723–725 (2006)
32. T.Y. Hsu, *Martensitic transformation and martensite* (Science, Beijing, 1999)
33. Z.Q. Kuang, J.X. Zhang, X.H. Zhang, K.F. Liang, P.C.W. Fung, Scaling behaviours in the thermoelastic martensitic transformation of Co. *Solid State Commun.* **114**, 231–235 (2000)